metal film. To maintain a sharp boundary with the OTS-covered region, a sufficiently large drop of the aqueous silver enhancer solution was placed on the hydrophobic portion of the surface (in the OTS-covered region) and then pushed with the tip of a pipette until being spontaneously and quantitatively sucked into the thiolated region, at the contact line between the two monolayer regions. This surface energy-driven phenomenon occurs because of the very high hydrophobicity (low surface energy) of the OTS (water contact angle ≈115°, advancing as well as receding), compared with that of the thiolated layer (advancing angle ≈60°, receding angle ≈30°). The development process was stopped, after a few minutes of exposure to the silver enhancer solution, by sucking most of the liquid with a piece of clean filter paper. Several rinses with drops of pure water were then performed in the same manner, starting from the OTS-covered region, the residual water on the silver film being let to evaporate under a dust cover. Weakly bound surface contaminants were finally removed with a piece of Scotch tape before taking the AFM images, without any visible damage being caused to the silver electrode or to its sharp boundary at the OTS-covered region.

Controlled self-assembly of silver micro- and nanofeatures on a monolayer template pattern produced by the direct lithographic action of the AFM tip (Figs. 3,4): the nanolithographic inscription of the –COOH pattern on OTS/Si is followed by loading of the patterned surface with Ag^+ ions (in the same manner as the Ag^+ loading of the thiolated surface (Figs. 2d,e) to produce the silver carboxylate salt). The reduction of the Ag^+ ions to elemental silver (yielding metallic silver nanoparticles and the regeneration of free –COOH surface groups) was done with hydrazine (N_2H_4) vapor, by placing the sample for ~10 min above a small beaker containing hydrazinium hydroxide ($N_2H_5^+OH^-$), in a closed glass vessel immersed in a water bath at ~40 °C [31]. The sample was finally rinsed in a water overflow and blown dry with clean nitrogen. The two-step silver generation cycle was repeated five times, after which the silver nanoparticles accumulated on the surface were mildly developed with a silver enhancer solution [23,24] (not shown). The nanowires connect the micron-size electrodes to the edge of a millimeter-size silver electrode (visible at the right side extremity of the images) fabricated by the process described in Figure 2.

Patterns were "written" with conductive W_2C-coated silicon tips (Silicon-MDT) in a controlled humidity atmosphere (65–70 % relative humidity, obtained by mixing dry and wet nitrogen), using contact mode raster lithography (minimal contact forces, 9–10 V positive sample bias relative to the tip, 3.5–3.7 ms/pixel). The AFM images were taken in the ambient atmosphere, in the semicontact mode, with regular silicon probes (Silicon-MDT). A SOLVER P47 instrument (NT-MDT, Moscow, Russia) was used for both patterning (with the lithographic software provided by the manufacturer) and imaging. Lateral conductivity images were obtained in the contact mode, as described in Figure 4.

Received: March 6, 2002
Final version: April 28, 2002

[1] *Nanoparticles and Nanostructured Films* (Ed: J. H. Fendler), Wiley-VCH, Weinheim **1998**.
[2] C. B. Murray, C. R. Kagan, M. G. Bawendi, *Annu. Rev. Mater. Sci*. **2000**, *30*, 545.
[3] A. C. Templeton, W. P. Wuelfing, R. W. Murray, *Acc. Chem. Res.* **2000**, *33*, 27.
[4] K. C. Grabar, K. J Allison, B. E. Baker, R. M. Bright, K. R. Brown, R. G. Freeman, A. P. Fox, K. D. Keating, M. D. Musick, M. J. Natan, *Langmuir* **1996**, *12*, 2353.
[5] M. M. Alvarez, J. T. Khoury, T. G. Schaaff, M. N. Shafigullin, I. Vezmar, R. L. Wetten, *J. Phys. Chem. B* **1997**, *101*, 3706.
[6] G. Markovich, C. P. Collier, S. E. Henrichs, F. Remacle, R. D. Levine, J. R. Heath, *Acc. Chem. Res.* **1999**, *32*, 415.
[7] L. F. Chi, M. Hartig, T. Drechsler, T. Schwaak, C. Seidel, H. Fuchs, G. Schmid, *Appl. Phys. A* **1998**, *66*, S187.
[8] G. Schmid, L. F. Chi, *Adv. Mater*. **1998**, *10*, 515.
[9] Y. Huang, X. Duan, Q. Wei, C. M. Lieber, *Science* **2001**, *291*, 630.
[10] C. Durkan, M. E. Welland, *Phys. Rev. B* **2000**, *61*, 14 215.
[11] C. Durkan, M. A. Schneider, M. E. Welland, *J. Appl. Phys.* **1999**, *86*, 1280.
[12] T. W. Ebbesen, H. J. Lezec, H. Hiura, J. W. Bennett, H. F. Ghaemi, T. Thio, *Nature* **1996**, *382*, 54.
[13] *Science and Application of Nanotubes* (Eds: D. Tománek, R. Enbody), Kluwer Academic/Plenum, New York **2000**.
[14] W. Fudickar, J. Zimmermann, L. Ruhlmann, J. Schneider, B. Röder, U. Siggel, J.-H. Fuhrhop, *J. Am. Chem. Soc.* **1999**, *121*, 9539.
[15] S. A. Levi, P. Guatteri, F. C. J. M. van Veggel, G. J. Vaneso, E. Dalcanale, D. N. Reinhoudt, *Angew. Chem. Int. Ed.* **2001**, *40*, 1892.
[16] A. N. Shipway, E. Katz, I. Willner, *ChemPhysChem* **2000**, *1*, 18.
[17] T. P. Cassagneau, B. Sweryda-Krawiec, J. H. Fendler, *MRS Bull.* **2000**, *25*, 40.
[18] Y. Lu, Y. Yang, A. Sellinger, M. Lu, J. Huang, H. Fan, R. Haddad, G. Lopez, A. R. Burns, D. Y. Sasaki, J. Shelnutt, C. J. Brinker, *Nature* **2001**, *410*, 913.
[19] V. Balzani, A. Credi, M. Venturi, in *Stimulating Concepts in Chemistry* (Eds: F. Vögtle, J. F. Stoddart, M. Shibasaki), Wiley-VCH, Weinheim **2000**, pp. 255–266.
[20] H. Ahmed, *J. Vac. Sci. Technol. B* **1997**, *15(6)*, 2101.
[21] J. R. Heath, *Acc. Chem. Res.* **1999**, *32*, 388.
[22] R. Maoz, S. R. Cohen, J. Sagiv, *Adv. Mater.* **1999**, *11*, 55.
[23] R. Maoz, E. Frydman, S. R. Cohen, J. Sagiv, *Adv. Mater.* **2000**, *12*, 424.
[24] R. Maoz, E. Frydman, S. R. Cohen, J. Sagiv, *Adv. Mater.* **2000**, *12*, 725.
[25] H. A. Lowenstam, S. Weiner, *On Biomineralization*, Oxford University Press **1989**.
[26] E. M. Landau, M. Levanon, L. Leiserowitz, M. Lahav, J. Sagiv, *Nature* **1985**, *318*, 353.
[27] S. Mann, B. R. Heywood, S. Rajam, J. D. Birchall, *Nature* **1988**, *334*, 692.
[28] E. M. Landau, S. Grayer Wolf, M. Levanon, L. Leiserowitz, M. Lahav, J. Sagiv, *J. Am. Chem. Soc.* **1989**, *111*, 1436.
[29] J. H. Fendler, F. C. Meldrum, *Adv. Mater.* **1995**, *7*, 607.
[30] J. Aizenberg, A. J. Black, G. M. Whitesides, *Nature* **1999**, *398*, 495.
[31] E. Frydman, *Ph.D. Thesis*, Weizmann Institute, September **1999**.
[32] W. J. Dressick, J. M. Calvert, *Jpn. J. Appl. Phys.* **1993**, *32*, 5829.

Ultralow-*k* Dielectrics Made by Supercritical Foaming of Thin Polymer Films**

By *Bernd Krause*, *Geert-Henk Koops*, *Nico F. A. van der Vegt*,* *Matthias Wessling*, *Michael Wübbenhorst*, and *Jan van Turnhout**

There is an urgent need for low- and ultralow-*k* dielectric materials. The present insulation materials such as silicon dioxide exhibit *k* values of 3.9–4.2) (*k* denotes the relative permittivity, which is often also symbolized by ε). Future generation materials require dielectric constants below 2.2.[1–3]

Non-polar polymers allow us to conquer the low-*k* region,[2,3] nonetheless only a few polymers meet the mechanical strength and temperature requirements. In the quest for lowering the permittivity of polymers down to ultralow-*k* values, several research groups are exploring the incorporation of nanosized air cells. Current initiatives are based on two principles: i) thermal decomposition of a block copolymer made of a thermally stable block and a thermally unstable one,[4–7] ii) thermolysis of high glass-transition temperature (T_g) polymers blended with thermally labile fillers (polymers or organic components).[8,9]

[*] Dr. N. F. A. van der Vegt, Dr. B. Krause,[+] Dr. G. H. Koops, Prof. M. Wessling
University of Twente, Membrane Technology Group
P.O. Box 217, NL-7500 AE Enschede (The Netherlands)
E-mail: n.f.a.vanderVegt@ct.utwente.nl
Prof. J. van Turnhout, Dr. M. Wübbenhorst
Delft University of Technology, Polymer Materials and Engineering
Julianalaan 136, NL-2628 BL Delft (The Netherlands)
E-mail: j.vanturnhout@tnw.tudelft.nl
[+] Present address: Gambro Dialysatoren GmbH & Co. KG, Membrane & Device Research, Holger-Crafoord-Str. 26, D-72379 Hechingen, Germany.

[**] M. Chalid and P. J. Droppert are gratefully acknowledged for assistance with the dielectric measurements.

  0935-9648/02/1508-1041 $ 17.50+.50/0

ADVANCED MATERIALS

An entirely different route reported on here introduces porosity in a physical and cleaner way. Our batch process invokes the foaming created by the evaporation of dissolved supercritical CO_2. This strategy has the following attractive features. Physical foaming by the escape of dissolved gases from a polymer is not only non-polluting; it also produces no impurities. It further enables precise tailoring of the morphology from microcellular[10] to bicontinuous, nanoporous structures.[11] It is feasible, starting from amorphous low-k rigid polyimides and by introducing porosities of up to 40 % to get well into the ultralow-k regime. In addition, by applying a mesoscopically ordered polymer we can create specially structured foams with disk-like pores, thus reducing the k-value even further into hitherto unknown areas of mechanically stable ultralow-k materials.

In our method[12] a thin polymer film is saturated with CO_2 at an elevated pressure. The saturated, swollen film is next removed from the pressure cell and immersed in a bath at an elevated temperature causing nucleation and growth of nanosized gas cells, which are dispersed uniformly throughout the film. By adjusting the conditions, the porosity of thin films, e.g., of high-T_g polyimides can be increased systematically, thus providing routes to tune the k-value at will.

Moreover, one may take advantage of the molecular order present in the polymer to control the shape of the voids, which in amorphous films usually is spherical. We will show that based on either amorphous or crystalline polyimides porous structures can be made with either cellular voids between 10 and 500 nm or with lamellar structures having interlayer distances below 100 nm. These porous materials all have dielectric constants in the ultralow-k range.

Five stiff, aromatic polyimides with different chemical composition and structure were studied; see Table 1. We selected two commercially available amorphous polyimides (**1**, **2**), two specially prepared 4,4′-(hexafluoroisopropylidene) diphthalic anhydride (6-FDA) based amorphous fluorinated polyimides (**3**, **4**), and commercially available semi-crystalline Kapton HN (**5**), see Experimental section. This selection was based

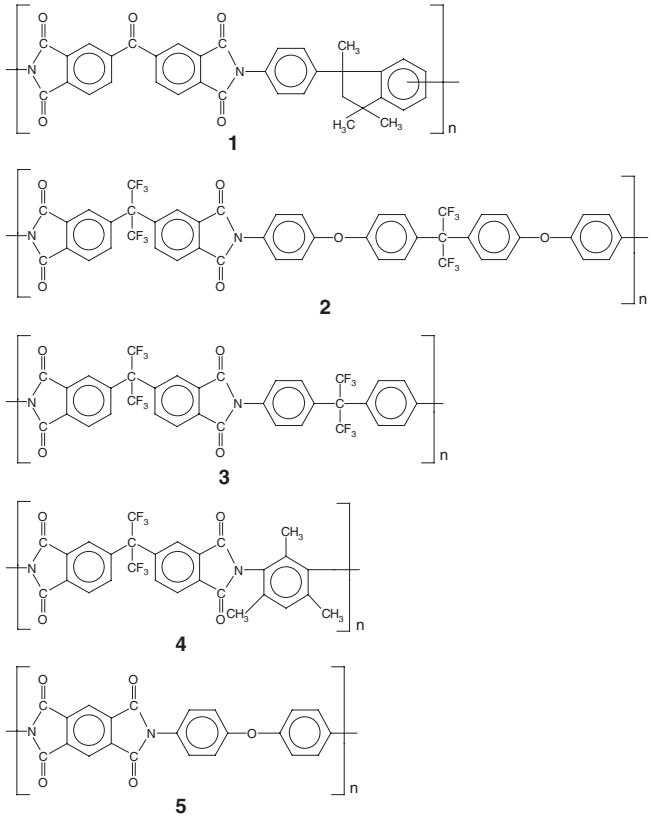

Table 1. Important process parameters of the pressure cell technique. The foaming experiments were performed for the given values of the process parameter.

Polymer	Foam No.	P_{sat} [MPa]	T_{sat} [°C]	T_{foam} [°C]	Morphology	Density [g/cm^3]	T_g [°C]	v_{air}	$\varepsilon'_{exp.}$ [a]	$\varepsilon'_{calc.}$ [c]	$\varepsilon'_{calc.}$ [d]
1					dense	1.240	314	0	3	3	3
	I	5.0	25	250	nanoporous	1.084		0.126	2.69	2.75	2.69
	II	5.0	25	270	nanoporous	0.914		0.263	2.18	2.47	2.37
	III	5.0	25	290	nanoporous	0.775		0.375	1.97	2.25	2.13
2					dense	1.430	250	0	2.79	2.79	2.79
	IV	5.5	25	220	microporous	1.207		0.156	2.4	2.51	2.45
	V	5.5	25	240	microporous	1.023		0.285	2.2	2.28	2.19
	VI[b]	5.5	0	240	nanoporous	0.861		0.398	1.87	2.08	1.97
3					dense	1.481	298	0	2.73	2.73	2.73
	VII	5.5	25	250	microporous	1.010		0.318	1.91	2.18	2.09
	VIII[b]	5.5	0	250	nanoporous	0.870		0.413	1.774	2.02	1.91
4					dense	1.343	395	0	2.574	2.57	2.57
	IX[b]	5.5	0	330	nanoporous	0.832		0.381	2.243	1.97	1.89
5					dense	1.45	380	0	3.15	3.15	3.15
	X	5.0	25	150	layered	1.35		0.069	2.85	3.00	2.96
	XI	5.0	25	200	layered	1.25		0.160	2.57	2.81	2.72
	XII	5.0	25	250	layered	1.13		0.221	2.26	2.67	2.57
	XIII	5.0	25	300	layered	1.08		0.255	1.98	2.51	2.39

[a] Measured at 1 kHz and 25 °C. [b] Saturation temperature reduced to 0 °C to compensate for higher carbon dioxide diffusivity in these materials and to increase solubility of carbon dioxide. [c] Using linear rule of mixtures. [d] Using Maxwell-Garnett's mean-field equation.

  0935-9648/02/1508-1042 $ 17.50+.50/0

on their low intrinsic dielectric constant, their thermal stability (reflected by a high glass-transition temperature) and differences in molecular packing, i.e., amorphous or semicrystalline.

Polymer films were prepared and saturated in a pressure cell at a CO_2-pressure P_{sat} and saturation temperature T_{sat}. Subsequently, the CO_2 was quickly released from the pressure vessel. The gas-saturated, plasticized polymer film was then immersed for 30 s in a heating bath that was held at the desired foaming temperature T_{foam}. The foamed samples were next quenched in ethanol and dried under vacuum at 30 °C to remove all traces of ethanol. The foam morphologies obtained depend mainly on the variables P_{sat}, T_{sat}, and T_{foam}.[11] The experimental conditions are presented in the Experimental section. The characteristic properties of the foamed polymers, such as T_g, densities, and dielectric constants are listed in Table 1.

During the transfer of the gas-saturated polymer from the pressure vessel to the heating bath, diffusion of carbon dioxide out of the polymer takes place. This leads to a lower carbon dioxide concentration near the surface and results in a dense skin layer, which covers the microporous foam core.

Figure 1 depicts the expansion of Matrimid (**1**) in terms of its mass density and shows the temperature window in which porous structures can be manufactured. The lower limit is the glass-transition temperature of the swollen polymer–gas mixture. It strongly depends on the carbon dioxide content. The upper limit is close to the glass-transition temperature of the neat polymer. At the maximum foaming temperature of 300 °C, the density of the foamed Matrimid (**1**) samples decreases to approximately 61 % of that of the initial polymer.

The porous Matrimid (**1**) films display a microcellular morphology with cell dimensions between 20 to 50 nm as shown in the scanning electron micrograph of Figure 2A. Such small cells have not been reported before for foaming techniques. The main reason for these extraordinary small cells is the high CO_2 solubility in Matrimid (**1**) and in polyimides in general, which causes very high gas nucleation densities.

Comparable porosities of 38, 40, 41, and 38 % could be achieved for all the amorphous polymers **1**–**4** investigated, at their maximum foaming temperature (Table 1). In all cases nanofoam structures were formed.

The saturation temperature (Table 1) can be utilized as an additional variable to control the void dimensions. Lowering the saturation temperature to 0 °C causes a significant increase in carbon dioxide solubility and at the same time a strong reduction in CO_2-diffusion out of the film. The large influence of the carbon dioxide content becomes apparent when we compare the scanning electron micrographs in Figures 2B and C. Microcellular morphologies prevail when the films are saturated at 25 °C, whereas nano-

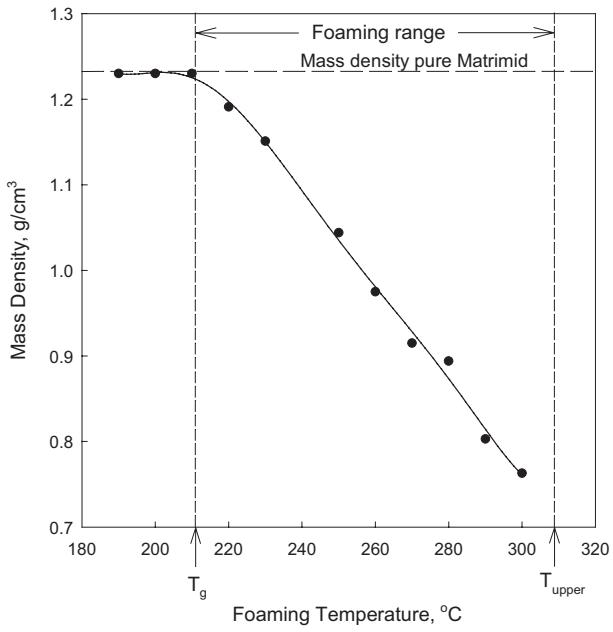

Fig. 1. Density of Matrimid (**1**) at different foaming temperatures. The samples were saturated with supercritical CO_2 (50 bar) for 2 h at room temperature. Foaming times of 30 s were used. Foaming starts at the glass-transition temperature (T_g) of the highly plasticized polymer/gas mixture and stops at an upper temperature (T_{upper}) close to the glass transition of the pure polymer.

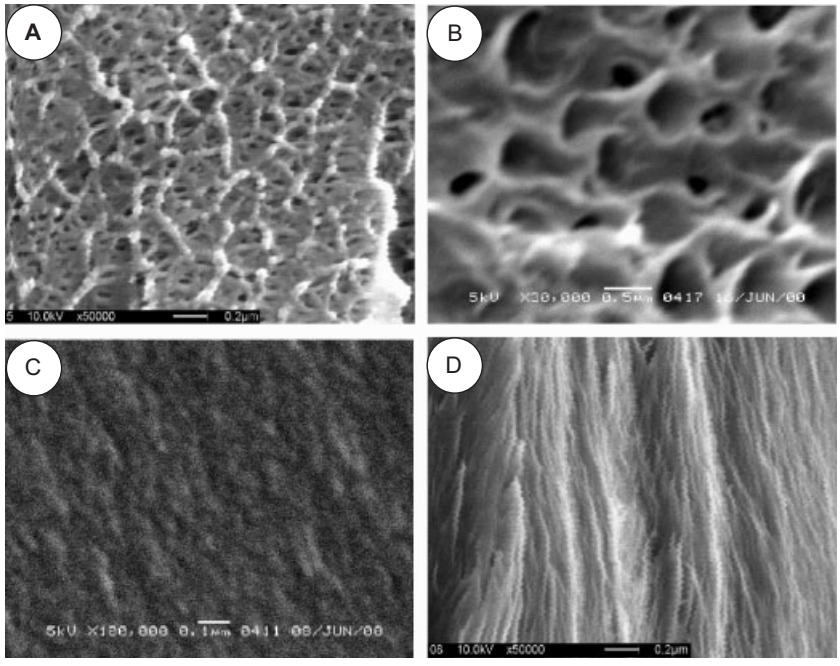

Fig. 2. SEM images: A) Matrimid (**1**) foamed at 270 °C. Magnification 50 000, white horizontal bar equals 200 nm. B) 6-FDA-4,4′-6F (**3**) saturated at 25 °C and foamed at 250 °C. Magnification 30 000, white horizontal bar equals 500 nm. C) 6-FDA-4,4′-6F (**3**) saturated at 0 °C and foamed at 250 °C. Magnification 100 000, white horizontal bar equals 100 nm. D) Kapton HN (**5**) foamed at 300 °C. Magnification 50 000, white horizontal bar equals 200 nm.

  0935-9648/02/1508-1043 $ 17.50+.50/0

ADVANCED MATERIALS

foam morphologies emerge when the carbon dioxide saturation step is performed at 0 °C. Only nanoporous structures (Fig. 2C) with pore sizes below 10 nm have the potential for application in multilayer microelectronic devices. For such applications continuous saturation and foaming steps have to be implemented.

For the characterization of the dielectric properties, see Experimental, we have studied all materials over a broad frequency (10^{-1}–10^{9} Hz) and temperature range (25–240 °C). The results confirm the expected: an advantageous marginal dependence of the permittivity on frequency and temperature owing to the low dielectric losses in all polyimides (see Fig. 3). For a comparison between polyimides (**1**–**4**) of varying porosity we can therefore restrict the discussion to values of the dielectric constant at 1 kHz and 25 °C, which are given in Figure 4 and in Table 1.

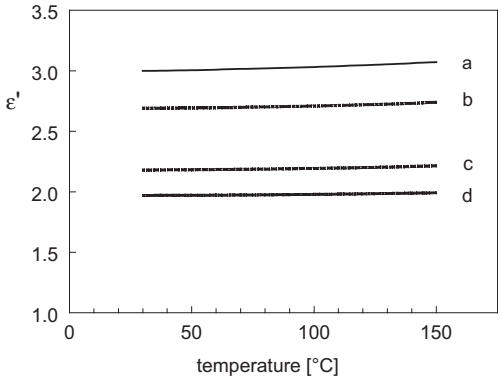

Fig. 3. Dielectric constant of the commercial PI (**1**) vs. temperature at 1 kHz, for 4 porosities: a) unfoamed, b) $v_{air} = 0.126$, c) $v_{air} = 0.285$, and d) $v_{air} = 0.375$.

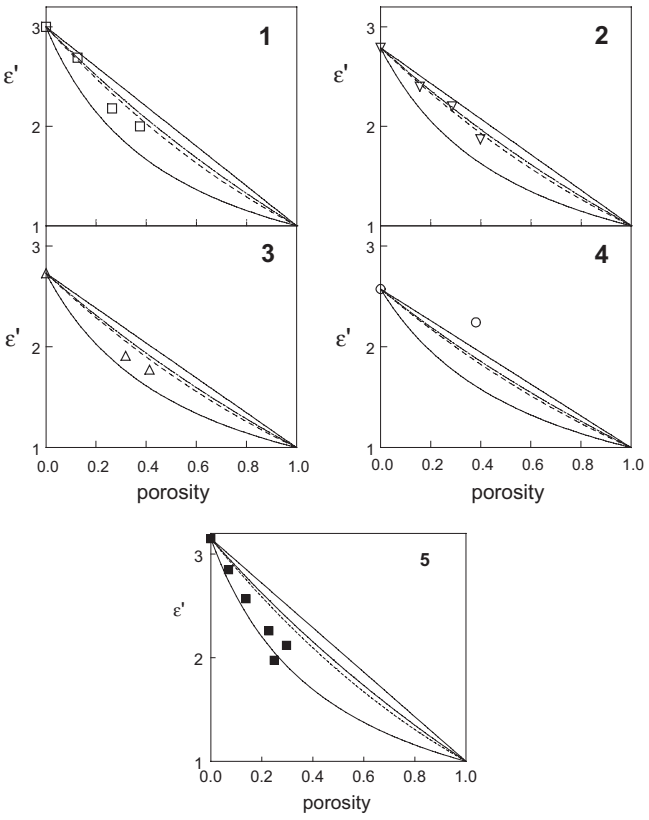

Fig. 4. Dielectric constant (ε' or k) vs. porosity for 5 types of aromatic polyimide nanofoams (**1**)–(**5**). The measured data are compared with predictions made with 4 rules of mixtures: parallel model – upper limit (full line), Maxwell–Garnett for spheres (dashed line), Looyenga–Landau–Lifshitz for spheres (dotted-dashed line), and series model – lower limit (full line).

As anticipated, all foams (samples I–IX in Table 1) show a considerable reduction in the dielectric constant. It drops down to $k = 1.77$ for the foamed materials. Interestingly, this is already below the ultralow-k limit.

Figure 4 shows for the amorphous polyimides (**1**–**4**), the relation between the porosity and the permittivity. The latter decreases noticeably as will be self-evident, since the increasing amount of air will ultimately lead to a permittivity of one.

We have modeled the measured permittivity of the two-phase nanofoams by two appropriate rules of mixtures. Both hold for spherical air inclusions ($\varepsilon_{air} = 1$) in a polymer matrix up to relatively high volume fractions, see Maxwell–Garnett (MG) and Looyenga–Landau–Lifshitz (LLL). The upper bound for k or ε vs. v_{air} (void fraction) calculated with the simple linear or parallel rule, and the lower bound, which corresponds to a layer or series model, are plotted as reference curves.

The measured k or ε vs. v_{air} data for three of the polyimides (**1**–**3**) roughly follow the curves for spherical inclusions. Interestingly, some ε-data drop below the MG and LLL-estimates, in particular for (**1**) and (**3**). This implies that the voids in these foams are flattened out to ellipsoids. This is beneficial, because it strengthens the lowering of k.

Polyimide (**4**), on the other hand, shows ε-values that surpass the upper bound. Such an odd behavior can only be rationalized by assuming a dielectric constant of the polyimide, ε_p, which unexpectedly rises with increasing porosity. A likely explanation for this undesired effect must be sought in the increased formation of charge transfer complexes (CTCs) as could be proved by fluorescence spectroscopy.[13]

Since CTCs are predominantly formed at higher temperatures, a too high foaming temperature (330 °C for sample IX) may result in more charge transfer complexes, which in turn enhance the electronic part of the dielectric constant of the polymer. CTCs have also been noticed by emission fluorescence for the polyimides (**2**) and (**3**). Such effects can fortunately be avoided by a proper choice of T_{foam}.

An even more profound reduction in the dielectric constant of polymers can be accomplished by reshaping the voids from spherical to disk-like. Unlike the other foaming techniques, which proceed from the amorphous polymer melt, supercritical solid-state foaming offers the unique opportunity to achieve this aim by increasing the aspect ratio of the voids drastically. By taking advantage of the molecular structure present in a polymer, we can thus come close to the lowest limit possible (series model).

In-plane oriented films, in which the molecular chains are aligned parallel to the film plane, are prone to expand normal to the thickness of the film. This provides the desired option

  0935-9648/02/1508-1044 $ 17.50+.50/0

to produce stratified foams. Layering occurs due to the affinity of carbon dioxide to the amorphous inter-crystalline regions. Owing to the rigid aromatic segments, the main chains in semi-crystalline Kapton HN (**5**) films are aligned parallel to the film plane,[14,15] making this polymer a suitable candidate.

Kapton HN (**5**) films were foamed at the conditions given in Table 1 and the dielectric properties of foams with different void fractions are presented in Figure 4. The drop in the dielectric constant with the void fraction shows a trend, which indeed follows the prediction for an ideal layer or series model. Clearly, a far more pronounced decrease in the dielectric constant is observed for (**5**) than for the amorphous polyimides (**1**–**4**) with spherical inclusions; k ($v_{air} = 0.255$) is already as low as 2.0 despite the high intrinsic dielectric constant of $k = 3.15$. This outcome is supported by the scanning electron micrographs of foamed (**5**) in Figure 2D, which clearly reveal a sheet-like structure. From these micrographs two characteristic layer spacings can be identified: a) distances between 1 and 10 nm, and (not shown) b) distances between 100 and 500 nm.

Foaming will not only reduce the dielectric constant, it will also lower the elastic modulus. We have measured the Young's modulus of non-foamed and foamed films of polymer (**2**) with the Perkin-Elmer 7e dynamic mechanical analyser in the temperature range from RT to 300 °C. All films showed the same temperature dependence with the modulus only falling slightly, until the glass transition was reached. Some values of the E-modulus at RT are collected in Table 2. The modulus drops roughly linearly with the porosity. Like the dielectric constant we have modeled the E-modulus too. We have used amongst others 3D-models, which allow the foams to be analyzed as co-continuous structures (not shown).

Table 2. Young's modulus of polymer (**2**) at RT vs. porosity.

Porosity	E-modulus [GPa]
0	2.1
0.156	1.7
0.285	1.3
0.398	1.0

We have presented a novel, versatile approach for the production of ultralow-k polymer films. Depending on the glass-transition temperature of the aromatic polyimide mechanically and thermally stable (> 300 °C) films are formed that have porosities of ca. 40 % and k or ε-values below 1.8. Molecular orientation of the parent polymers allows one to manipulate the foam morphology from spherical to layered structures, which yield the lowest k-values realizable.

The nanofoams are not only of importance for ultralarge-scale integration on chips, they also represent a new family of materials for the long term storage of electrical charges in polymers. As such they might spur a new breed of electret devices, including the piezo and pyro-active ones.[16–18]

A variety of other options can be pursued using supercritical foaming. We foresee, for instance, that polymers that tend to self-organize in aligned mesoscopic structures—such as side-chain or main-chain liquid crystalline polymers—might allow us to boost the porosity to even higher values (like those in aero- and xerogels) without sacrificing the mechanical strength.

Experimental

Materials: Matrimid 5218 (**1**) and LaRC-CP1 (**2**) were obtained from Ciba Specialty Chemicals, Basel, Switzerland and SRS Technologies, Huntsville, USA, respectively. The 6-FDA based polyimides 6-FDA-4,4′-6F (**3**) and 6-FDA-TMPD (**4**) were synthesized by chemical imidization of the poly(amic acid) precursor. The poly(amic acids) of both fluorinated polyimides were prepared from equimolar amounts of 4,4′-(hexafluoroisopropylidene) diphthalic anhydride (6-FDA) and the corresponding diamine (2,2-bis(4-aminophenyl) hexafluoropropane (4,4′-6F) and 2,4,6-trimethyl-1,3-phenylenediamine (TMPD)) by solution condensation in *N*,*N*-dimethylacetamide. The poly(amic acid) precursors were converted to the corresponding polyimides by chemical imidization with acetic anhydride and pyridine. The 6-FDA based polyimides were precipitated in methanol and purified by dissolving in *N*,*N*-dimethylformamide and precipitation in methanol again. Kapton HN (**5**) films of 75 μm were obtained from DuPont, USA and used as received.

Foam Formation: The polymers (**1**–**4**) shown in Table 1 are used for film formation (~ 100 μm thick) by solution casting (20 wt.-% polyimide in *N*-methylpyrrolidone) on a glass plate. The cast films were dried in a nitrogen atmosphere at 75 °C for 4 h. Subsequently, the homogeneous dense films were removed from the glass and further dried under vacuum at 150 °C for several weeks to remove the last traces of solvents. Commercially Kapton HN (**5**) films of 75 μm were dried under vacuum at 150 °C for 2 days. The polymer films (**1**–**5**) were cut into 4 cm × 4 cm pieces and placed in a pressure vessel connected to a carbon dioxide cylinder. The samples were then saturated with carbon dioxide at a saturation temperature (T_{sat}) and saturation pressure (P_{sat}) for 2 h (saturation half-times scale with the square of the film thickness and are significantly lower for thinner films). Subsequently, the carbon dioxide was quickly released from the pressure vessel (within 1 s). After removing the gas-saturated polymer film from the pressure vessel, the sample was immersed for 30 s (foaming time) in a glycerol bath maintained at the desired foaming temperature (T_{foam}). The foamed samples were next quenched in an ethanol/water (50:50) mixture, washed in ethanol, and dried under vacuum at 30 °C for 24 h to remove traces of ethanol and water.

Characterization Methods: The glass-transition temperature, T_g, of the films was determined with a Perkin Elmer differential scanning calorimeter DSC7, using the second heating run at a rate of 20 K min^{-1}. The density of the films and foams were determined by applying the flotation weight loss method (ASTM D-792) with hexane as liquid. The void fraction (v_{air}) was calculated from the density data.

The microcellular morphologies of the foamed samples were investigated using a Joel JSM-5600 LV scanning electron microscope (SEM). The samples were freeze fractured in liquid nitrogen and sputter coated (Balzers/Union 040) with gold at an argon pressure of 13 Pa for 2 min at a current of 14 mA.

Dielectric properties of the well-dried film samples were measured by a broadband dielectric spectrometer using a combination of three dielectric analyzers for (partially) overlapping frequency ranges: a frequency response analyzer (Schlumberger 1260) with a custom-made dielectric interface (10^{-2}–10^{4} Hz), a Hewlett-Packard 4284 A precision LCR-meter (10^{2}–10^{6} Hz) and a HP4194 A RF-spectrometer (10^{6}–1.8×10^{9} Hz). For the dielectric analysis, squared pieces were cut from the films. On both sides of the pieces Au electrodes ($\phi = 20$ mm) were sputtered to provide good electrical contact to the plate electrodes of the cryostat. Careful measurement of the thickness and area of the samples, together with calibrations of the electrode and analyzer configuration, resulted in k values with an error of 3 % or less.

The following equations were used for the computations:

$$\text{parallel - upper limit: } \varepsilon' = 1 + v_p\,(\varepsilon'_p - 1) \quad (1)$$

$$\text{series - lower limit: } 1/\varepsilon' = 1 + v_p\,(1/\varepsilon'_p - 1) \quad (2)$$

$$\text{Maxwell-Garnett - spheres: } (\varepsilon' - 1)/(\varepsilon' + 2) = v_p\,(\varepsilon'_p - 1)/(\varepsilon'_p + 2) \quad (3)$$

$$\text{LLL - spheres: } \varepsilon'^{1/3} = 1 + v_p\,(\varepsilon'^{1/3}_p - 1) \quad (4)$$

where ε' is the real part of the dielectric constant of the foam, ε'_p that of the polymer and v_p the volume fraction of the polymer. Since the losses are small,

  0935-9648/02/1508-1045 $ 17.50+.50/0

ADVANCED MATERIALS

we could simply use the real part ε' in all models. Note that k equals ε', and that $\varepsilon'_{air} = 1$. For theoretical details about the models, see, e.g., C. J. F. Böttcher and P. Bordewijk [19]. For non-spherical voids, as is the case for (**1**) and (**3**), the MG and LLL-models should be modified by introducing a shape factor. This shape factor is determined by the aspect ratio; for spheres it equals 1/3, see, e.g., G. Banhegyi [20].

Received: March 4, 2002
Final version: May 1, 2002

[1] R. D. Miller, *Science* **1999**, *286*, 421.
[2] *Handbook of Low and High Dielectric Constant Materials and Their Applications*, Vol. 1–2 (Ed. H. S. Nalwa), Academic Press, San Diego, CA **1999**.
[3] G. Maier, *Prog. Polym. Sci.* **2001**, *26*, 3.
[4] O. Gain, G. Seytre, J. Garapon, J. Vallet, B. Sillion, in *ACS Meeting: High-Temperature Properties and Application of Polymeric Materials*, Vol. 603, American Chemical Society, Washington, DC **1994**, p. 201.
[5] D. W. Kim, S. S. Hwang, S. M. Hong, H. O. Yoo, S. P. Hong, *Polymer* **2001**, *42*, 83.
[6] S. Mikoshiba, S. Hayase, *J. Mater. Chem.* **1999**, *9*, 591.
[7] J. L. Hedrick, K. R. Carter, J. W. Labadie, R. D. Miller, W. Volksen, C. J. Hawker, D. Y. Yoon, T. P. Russell, J. E. McGrath, R. M. Briber, *Adv. Polym. Sci.* **1999**, *141*, 1.
[8] T. Takeichi, M. Zuo, A. Ito, *High Perform. Polym.* **1999**, *11*, 1.
[9] Y. Xu, Y. Tsai, K. N. Tu, B. Zhao, Q.-Z. Liu, M. Brongo, G. T. T. Sheng, C. H. Tung, *Appl. Phys. Lett.* **1999**, *75*, 853.
[10] a) V. Kumar, J. E. Weller, *Int. Polym. Processing* **1993**, *8*, 73. b) V. Kumar, *Cell. Polym.* **1993**, *12*, 207. c) S. K. Goel, E. J. Beckman, *Cell. Polym.* **1993**, *5*, 11. d) K. A. Arora, A. J. Lesser, T. J. McCarthy, *Macromolecules* **1998**, *31*, 4614. e) C. M. Stafford, T. P. Russell, T. J. McCarthy, *Macromolecules* **1999**, *32*, 7610.
[11] B. Krause, H. J. P. Sijbesma, P. Münüklü, N. F. A. van der Vegt, M. Wessling, *Macromolecules* **2001**, *34*, 8792.
[12] B. Krause, R. Mettinkhof, N. F. A. van der Vegt, M. Wessling, *Macromolecules* **2001**, *34*, 874.
[13] H. Tang, H. Feng, H. Luo, L. Dong, Z. Feng, *Eur. Polym. J.* **1997**, *33*, 519.
[14] H. Hatori, Y. Yamada, M. Shiraishi, *Carbon* **1992**, *30*, 763.
[15] N. Takahashi, D. Y. Yoon, W. Parrish, *Macromolecules* **1984**, *17*, 2583.
[16] J. van Turnhout, R. E. Staal, M. Wübbenhorst, P. H. de Haan, *Proc. 10th Int. Symp. on Electrets*, IEEE Service Center, Piscataway, NJ **1999**, p. 785.
[17] R. Gerhard-Multhaupt, W. Künstler, T. Görne, A. Pucher, T. Weinhold, M. Seisz, *IEEE Trans. Diel. Electr. Insul.* **2000**, *7*, 480.
[18] G. M. Sessler, *J. Electrostat.* **2001**, *51*, 137.
[19] a) *Theory of Electric Polarazation*, 2nd ed., Vol. 2 (Eds: C. J. F. Böttcher, P. Bordewijk), Elsevier, Amsterdam **1978**. b) *Dielectric Properties of Heterogeneous Materials* (Ed: A. Priou), Elsevier, Amsterdam **1992**. c) P. A. M. Steeman, J. van Turnhout, in *Broadband Dielectric Spectroscopy* (Eds: F. Kremer, A. Schönhals), Springer, Berlin **2002**.
[20] G. Banhegyi, *Colloid Polym. Sci.* **1986**, *264*, 1030.

Uniform Boron Nitride Coatings on Silicon Carbide Nanowires**

By *Chengchun Tang*,* *Yoshio Bando*,* *Tadao Sato*, and *Keiji Kurashima*

Research into one-dimensional nanometer-scale structures is at present attracting considerable interest due to their contribution to the understanding of basic concepts and potential technological applications.[1] Among the various interesting novel materials, SiC nanowires are of technological relevance especially for their potential applications in nanoelectronics, nanocomposites, and electron field-emitting devices.[2] Mechanical properties measured by combining atomic force microscopy and lithography techniques indicate that the strength of SiC nanowires is a factor of two times better than observed previously for SiC whiskers of micrometer diameter. SiC nanowires, therefore, are excellent candidates for reinforcing elements in composites.[3] In fact, there has been a great deal of research in reducing failure of brittle matrices by incorporation of SiC whiskers. Depending on the nature of SiC whisker and matrix, strong whisker/matrix interactions usually are inevitable and the strength of the composite structure is therefore not significantly improved over the strength of the pure matrix.[4] The SiC nanowires should also show an interaction with the matrix due to the fine structure and high surface area. Considering that whisker/matrix interfacial properties can be weakened by using whiskers that are coated by chemically stable boron nitride,[5] boron nitride coatings on SiC nanowires might offer an effective approach to depressing the interaction because BN has unique chemical and physical properties such as low density, high melting point, chemical inertness, and high thermal conductivity in a wide range of temperatures. This type of coating should also be valuable for using the nanowires as a separate layer between semiconductor nanowires and electronic substrates due to the insulating nature of boron nitride,[6] and as a promoting component for large field-emitting factors due to its negative electron affinity.[7]

SiC nanowires (nanorods) have been fabricated by carbon nanotubes-confined reactions,[8] catalytic[2c] or hot-filament assisted[9] chemical vapor deposition, and arc-discharge[10] methods. Amorphous silica,[11] boron nitride nanotubes,[12] or boron nitride–carbon wrappers[13] (nanocables) on SiC nanowires have also been synthesized. However, the mentioned processes are usually expensive and do not provide uniform coatings over the entire surface of the nanowires. The poorly crystallized and non-uniform coatings adversely affect the thermomechanical and electronic properties of the composites.

Our process described here produced SiC nanowires that were uniformly coated with boron nitride by a specially designed chemical reaction to control the relative concentration of boron nitride and silicon carbide and to simultaneously generate their gas-phase precursors for chemical vapor deposition. B_2O_2 and SiO vapors were generated by heating the mixture of boron and silicon oxide at the high temperature of 1500 °C by the following solid-state reaction:

$$2B(s) + 2SiO_2(s) \longrightarrow B_2O_2(g) + 2SiO(g) \quad (1)$$

The simultaneously formed vapors were transported to a deposition area, where a highly oriented pyrolitic graphite (HOPG) covered with fine nickel catalyst grains was placed. Silicon carbide and boron nitride can be formed on the sur-

[*] Dr. C. C. Tang, Prof. Y. Bando, T. Sato, K. Kurashima
Advanced Materials Laboratory, National Institute for Materials Science
1-1 Namiki, Tsukuba, Ibaraki 305-0044 (Japan)
E-mail: Tang.Chengchun@nims.go.jp

[**] C. T. thanks F. Xu and Y. Gao for their help with the TEM characterization.

  0935-9648/02/1508-1046 $ 17.50+.50/0